





RESEARCH ARTICLE OPEN ACCESS

Building Single-Atom and Single-Cluster Metal Catalysts Supported on Graphdiyne and Boron-Graphdiyne

Johanna Sandoval Menjivar¹  | Estefanía Germán¹  | Julio A. Alonso^{1,2}  | María J. López¹ ¹Departamento de Física Teórica, Atómica, y Óptica, University of Valladolid, Valladolid, Spain | ²Donostia International Physics Center (DIPC), San Sebastián, Spain**Correspondence:** María J. López (mariajlopez@uva.es)**Received:** 31 July 2025 | **Revised:** 30 October 2025 | **Accepted:** 3 November 2025**Keywords:** activation barriers | boron-graphdiyne layers | DFT | diffusion of atoms | graphdiyne layers | single-atom catalysts | single-cluster catalysts

ABSTRACT

Transition metal (TM) atoms and clusters supported on layered materials can be used to build single-atom (SAC), and single-cluster catalysts (SCC), respectively. To gain insight and to contribute to the rational design of SACs and SCCs, we investigate the structure and stability of SACs and SCCs of V, Co, and Pd, built on two supports, graphdiyne (GDY) and boron-graphdiyne (BGDY), using the density functional formalism. GDY and BGDY are carbon-based layered materials exhibiting a structure of uniformly distributed nanopores. The triangular pores of GDY and the hexagonal pores of BGDY host TM atoms and clusters attached with high adsorption energies, favoring the stability of these systems. Diffusion of metal atoms on GDY and BGDY is hindered by large activation barriers preventing the aggregation of atoms. Adsorption of metal atoms (one, two or three atoms per cell) or clusters (one TM₆ per cell) induce global distortions in the hexagonal lattice of BGDY. However, the GDY lattice is more robust and its global structure is quite insensitive to metal doping. Local distortions of the carbon chains are observed in both layers in the proximity of the adsorbed atoms and clusters. This work gives support to the development of highly stable SACs and SCCs that can be built through deposition of TM atoms and clusters on GDY and BGDY.

1 | Introduction

Nowadays, catalysis plays a very important role in different industrial processes, as it allows accelerating the speed of a chemical reaction without altering the final product. This facilitates large-scale production of valuable chemicals by decreasing the required energy. Since 90% of the products synthesized in the chemical industry are obtained by catalytic processes [1], this is a subject of considerable interest. Transition metals (TM) perform as excellent catalysts in many reactions [2–4] of homogeneous and heterogeneous catalysis, because of their unfilled d-shells, different oxidation states, and good selectivity and activity. An application that generates much interest is the synthesis and storage of hydrogen. Being hydrogen a potential supply of clean energy, this can help to replace fossil fuels and thereby reduce CO₂ emissions. One of the well-studied methods of H₂ production is the Hydrogen

Evolution Reaction (HER) [5], which requires the use of catalysts. Platinum, palladium, rhodium, ruthenium, iridium, and osmium, which form the so-called platinum-group metals (PGMs) [6] in metallurgy, are emerging as good catalysts for this purpose, but their use for industrial scale applications is expensive. Vanadium, cobalt, and palladium are transition metals of the 5th, 9th and 10th groups of the periodic table, respectively, which have been employed as catalysts in different processes [7–9] and have attracted attention for their use in HER [10–12]. Palladium has a lower cost than Pt and comparable performance [12]. According to Gupta et al. [11], 90% of the produced cobalt is used as catalyst in industry. Vanadium, on the other hand, has been used for decades in ammonia-based selective catalytic reduction [13].

Supported TM catalysts have been intensively investigated [14, 15]. A good choice for a support platform can help to

This is an open access article under the terms of the [Creative Commons Attribution](https://creativecommons.org/licenses/by/4.0/) License, which permits use, distribution and reproduction in any medium, provided the original work is properly cited.

© 2025 The Author(s). *Small Structures* published by Wiley-VCH GmbH.

improve the catalytic efficiency due to the metal–support interaction. One of the reasons for using supports is to reduce the amount of catalyst needed, while retaining the catalytic performance. This is attributed to the fact that the support helps keeping the catalyst in a dispersed state [16]. Catalytic activity and selectivity can be adjusted by varying the size of the metal nanoparticles. In addition, since catalysis occurs at the surface of the nanoparticle, decreasing the size of the nanoparticles as much as possible is desirable. Many studies have been performed in this topic [17–19] showing the size dependence of the catalytic performance, in particular, studies of single-atom catalysis (SAC) and single-cluster catalysis (SCC). Work on SAC was initiated in 2011 by Qiao et al. [20], when they built a catalyst formed by single Pt atoms dispersed on a FeO_x support. Carbon-based materials are proposed as efficient support platforms for catalysis due to their excellent electronic and mechanical properties, high superficial area, and low cost [21, 22]. The porosity of these materials serves to anchor metal atoms and clusters. A strong binding between the TM and the support becomes extremely important, because it prevents the diffusion of the metal atoms through the support, while a weak interaction may allow the aggregation of metal atoms.

Graphdiyne (GDY) [23] and boron-graphdiyne (BGDY) [24] are novel layered carbon materials which have become attractive for their use in catalysis and energy applications [25, 26]. Based on this interest, we have performed density functional theory (DFT) calculations to investigate the adsorption of TM atoms (V, Co, Pd) on GDY and BGDY, and how the metal–support interaction affects the structure of these systems. Adsorption of one, two, and three TM atoms, as well as six-atom clusters on both layered substrates, was investigated. The structures obtained, and their stabilities, provide relevant information and support for the building of SAC and SCC catalysts platforms. V, Co, and Pd provide a balanced selection including early (V) and late (Co, Pd) TMs of the 3d (V, Co) and 4d (Pd) rows, and in addition, there is evidence of the catalytic activity of these metals [7–13].

2 | Results

GDY and BGDY belong to a family of carbon-based layered materials exhibiting a nanoporous structure. The triangular pores of GDY are bounded by diacetylenic chains linking carbon hexagons sitting on the corners of the triangles. BGDY has hexagonal pores in which boron atoms on the corners of the hexagons are linked by diacetylenic chains. The GDY layer was modeled as a repetitive supercell consisting of 72 C atoms (4-unit cells) and the BGDY layer was modeled as a repetitive cell containing 12 C atoms and 2 B atoms. The fully relaxed structures and supercells of GDY and BGDY are shown in Figure 1. The length of the cells in the z direction (perpendicular to the layer plane) was fixed at 14 Å for GDY, and 20 Å for BGDY, large enough to avoid interaction between periodic images. More details have been given by German and coworkers [27].

To study the metal–support interaction, calculations were performed in which the cell parameters (\vec{a} , \vec{b} , and γ) were allowed to vary along with the optimization of the positions of all the atoms in the cell. To model SACs, we start by adsorbing one

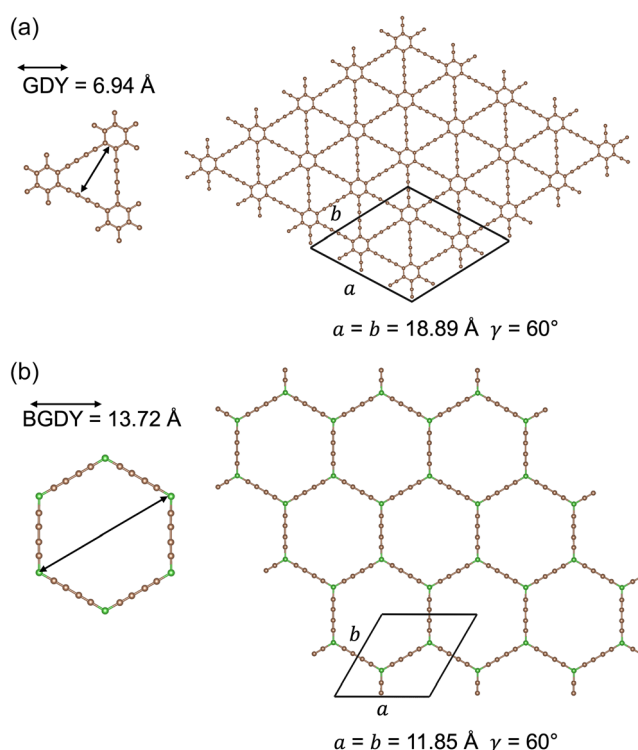


FIGURE 1 | Optimized structures of GDY and BGDY layers. Unit cells used in the calculations are delineated, and the cell parameters a , b , and γ (angle between \vec{a} and \vec{b}) are given in the figure. (a) GDY layer; the supercell contains 72 C atoms. (b) BGDY layer; the unit cell contains 12 C atoms and 2 B atoms. B atoms are represented in green color. Measures of the size of the triangular pores of GDY and the hexagonal pores of BGDY are indicated in the insets.

metal atom per unit cell. Next, the coverage is increased by adsorbing two and three atoms per cell, in order to investigate the stability of the single atom configuration and the chances of aggregation. The diffusion barriers of the metal atoms, relevant for the stability of the SACs, are also determined. To study SCCs, six-atom clusters were adsorbed on both layers.

2.1 | Adsorption of Transition Metal Atoms on GDY

The preferential sites for adsorption of a single V, Co, or Pd atom on GDY are the corners of the triangular holes. The atom is placed between the two carbon chains forming the sides of the corner (Figure 2), building bonds with two C atoms of each chain. Full relaxation of the cell parameters (a , b , γ) of the TM-GDY system produces no significant changes in the form of the unit cell: only changes of 0.2% in a and b , and 0.07% in γ . Adsorption occurs without visible local changes of the GDY structure, and only minor distortions of the carbon chains occur near the metal atom. The adsorption energy of a TM atom was obtained as:

$$E_{\text{ads}}(\text{TM-GDY}) = E(\text{GDY}) + E(\text{TM}) - E(\text{TM-GDY}) \quad (1)$$

where $E(\text{GDY})$ is the energy of a clean layer, $E(\text{TM})$ is the energy of an isolated metal atom, and $E(\text{TM-GDY})$ is the energy of the

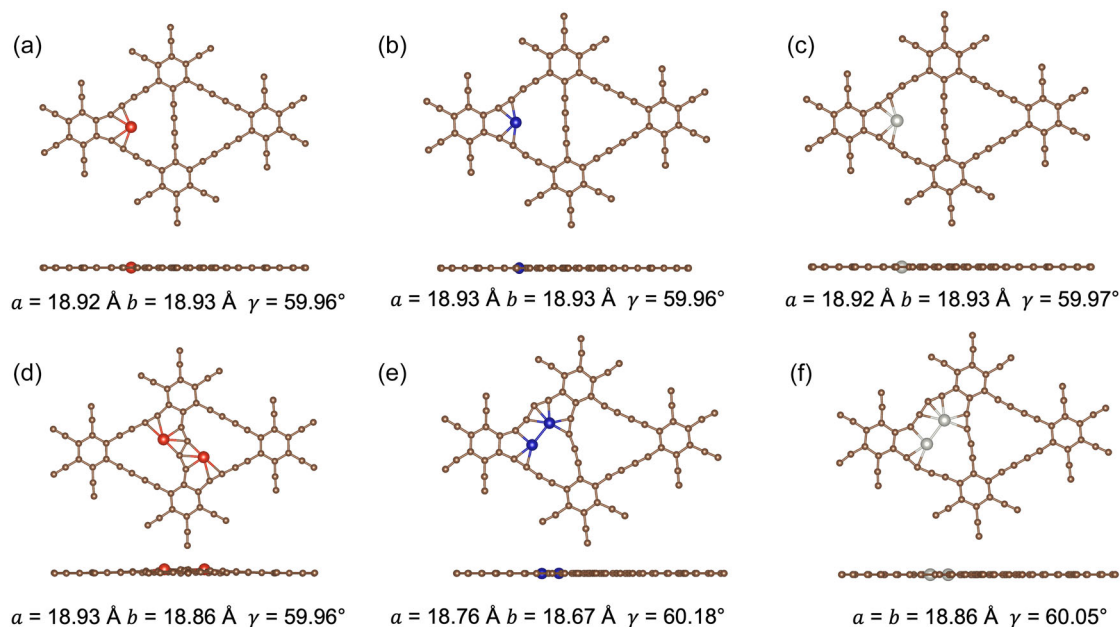


FIGURE 2 | Upper panel: front and side views of the most stable configuration of a TM atom adsorbed on GDY: (a) V, (b) Co, and (c) Pd. V is shown in red, Co in blue, and Pd in gray color. Lower panel: similar plots for the most stable configuration of two adsorbed TM atoms: (d) 2V, (e) Co₂, and (f) Pd₂. In all cases, a , b , and γ lattice parameters of the optimized cells are indicated.

layer with the TM atom adsorbed. Positive values of E_{ads} indicate exothermic adsorption. A similar equation applies for the adsorption of TM atoms on BGDY (see below). Adsorption energies of the three metal atoms on GDY are high (Table 1). Pd has the lowest adsorption energy, 2.65 eV, while V and Co have similar adsorption energies of 3.55 eV. These values can be compared with the adsorption energies on graphene, which are 1.93 (V) [28], 0.32 eV (Co) [29], and 1.09 eV (Pd) [30]. The binding of the metal atoms to GDY is larger, and the high values give confidence that GDY may serve as an efficient support for SACs.

The GDY layer can be decorated with a second TM atom, which can be adsorbed on several positions, relative to the first one. Figure S1 shows the eleven nonequivalent configurations of the two atoms in the cell. The adsorption energy of the second TM atom is

$$E_{\text{ads}}(2^{\text{nd}} \text{ atom}) = E(\text{TM-GDY}) + E(\text{TM}) - E(2\text{TM-GDY}) \quad (2)$$

where $E(2\text{TM-GDY})$ is the energy of GDY with two atoms adsorbed. The adsorption energies of the second TM atom for the relaxed structures corresponding to the 11 nonequivalent configurations are given in Table S1. The most stable configurations for two V, two Co, and two Pd atoms are shown in Figure 2.

TABLE 1 | Adsorption energies (in eV) of a single transition metal atom on GDY (per cell). Metal-carbon bond lengths $d(\text{TM-C})$ are given in Å.

System	E_{ads}	d (TM-C)
V-GDY	3.55	2.08–2.13
Co-GDY	3.55	1.90–1.94
Pd-GDY	2.65	2.06–2.18

Two Co (two Pd) atoms are adsorbed preferentially at two corners of the same triangular hole, resulting in the clustering of a Co₂ (Pd₂) dimer. In contrast, two V atoms are adsorbed on two touching triangular holes, at the two sides of the common carbon chain, in nonadjacent corners. Those two configurations are competitive for two adsorbed TM atoms, as one can notice in Table S1, specially for Pd. Table 2 shows the adsorption energies of the second TM atom, and some structural parameters of the lowest energy configurations with two V, two Co, and two Pd atoms adsorbed.

The adsorption energy of two TM atoms is calculated as:

$$E_{\text{ads}}(\text{two atoms}) = 2E(\text{TM}) + E(\text{GDY}) - E(2\text{TM-GDY}) \quad (3)$$

The adsorption energy of two V atoms forming a V₂ dimer on the same triangular pore is 7.67 eV, and in the case of two V atoms adsorbed on adjacent pores in the configuration of Figure 2, the adsorption energy is 7.99 eV. That is, the nondimerized configuration is 0.32 eV more stable. In the nondimerized configuration, the adsorption energy of the second V atom is 4.44 eV, which is 0.89 eV higher than the adsorption energy of the first V atom (3.55 eV). At first sight, it may surprise that the two V atoms do not form a dimer. The preference for the nondimerized

TABLE 2 | Adsorption energies of the second TM (V, Co, and Pd) atom on GDY as defined by (Equation 2), for the respective lowest energy configurations. Interatomic distances in Å.

System	E_{ads} (eV)	d (TM-C)	d (TM-TM)
2V-GDY	4.44	1.93–2.25	3.95
Co ₂ -GDY	4.11	1.86–2.11	2.45
Pd ₂ -GDY	2.76	2.03–2.23	2.58

configuration emerges because the measured bond length in free V_2 is 1.77 Å [31, 32], a short bond length. Interestingly, when the two V atoms are adsorbed at two corners of the same triangular pore, the calculated distance between the two V atoms is 2.61 Å, that is, those two atoms are far apart and cannot profit from V–V bonding. The preferred alternative is that the carbon chain common to two adjacent pores deforms to optimally accommodate the two V atoms, one on each pore. The parameters (a , b , γ) of the fully relaxed GDY supercell with the two adsorbed V atoms do not change significantly with respect to the cell of the pristine GDY layer. There is, however, a local deformation of the carbon chain hosting the two V atoms. That deformation has an energetic cost, but is compensated by the optimized binding of the V atoms to the chain. Formation of Co_2 is more stable than dispersion of two atoms in adjacent pores (see the adsorption energies of the second atom in Table S1). The differences in adsorption energy range between 0.32 and 1.0 eV. The dimerized Co atoms are at a distance of 2.45 Å, not far from the experimental bond length of 2.31 Å in free Co_2 [33]. In the dimer configuration, the Co atoms take profit of Co–Co bonding without compromising the Co–C bonds. In fact, the adsorption energy of the second Co atom, 4.11 eV, is higher than the adsorption energy of the first Co atom (3.55 eV) due to Co–Co bonding. The presence of the Co dimer deforms locally the carbon chains of the triangular pore, but the layer maintains planarity, and only minor changes of the cell parameters occur. Formation of Pd_2 adsorbed on a single pore is almost degenerate (10 meV more stable) with configurations in which the two Pd atoms are dispersed in adjacent pores. The distance between the two dimerized Pd atoms, 2.58 Å, is close to the calculated bond length of free Pd_2 , which is 2.54 Å [34], or 2.52 Å [35]. Moreover, the adsorption energy of the second Pd atom, 2.76 eV, is only 0.11 eV higher than the adsorption energy of the first Pd one (2.65 eV). These features reveal competition between formation of Pd–Pd and Pd–C bonds. Some deformation of the carbon chains in contact with the Pd atoms is observed, but there are no significant changes in the global GDY cell.

Several configurations have been investigated for the decoration of GDY with three adsorbed TM atoms, and the results are reported in Section S2. The lowest energy configurations show the three adsorbed atoms forming a triangle inside a pore (Figure S3). By comparing the adsorption energies of the third adsorbed atom, given in Table S3, with those for the first and second adsorbed atoms in Tables 1 and 2, one can notice that rising TM coverage leads to an increase of the adsorption energy of the last adsorbed atom. This increase is associated with the formation of metal–metal bonds.

2.2 | Diffusion of Transition Metal Atoms on GDY

The adsorption energies of V, Co, and Pd atoms on GDY are large, which is the first premise for the development of supported SACs. However, the formation of dimer and trimer clusters on GDY is energetically preferred over decoration of the layer with single, well-separated atoms (exception made of two V atoms). Therefore, the diffusion of the metal atoms leading to aggregation is an issue of great relevance for the stability, and lately the performance of SACs on GDY. We have performed nudged-elastic-band (NEB) [36] calculations to investigate the activation barriers for diffusion. Figure 3 shows the barriers for diffusion of one V, Co, and Pd atom, respectively, from its lowest energy configuration in one corner of a pore to an equivalent position in an adjacent corner of the same pore. High barriers, 1.61 and 1.04 eV, are present for the diffusion of Co and Pd atoms, respectively. These high barriers would prevent the diffusion under ambient conditions (or even at higher temperatures) of well-dispersed Co and Pd atoms on GDY. But the barrier for diffusion of V atoms, 0.24 eV, is not high enough to prevent diffusion of V atoms at room temperature. The lower limit to avoid significant diffusion at room temperature is usually established around 0.5 eV.

The diffusion of metal atoms from one pore to an adjacent pore already occupied by another metal atom to form a dimer was also

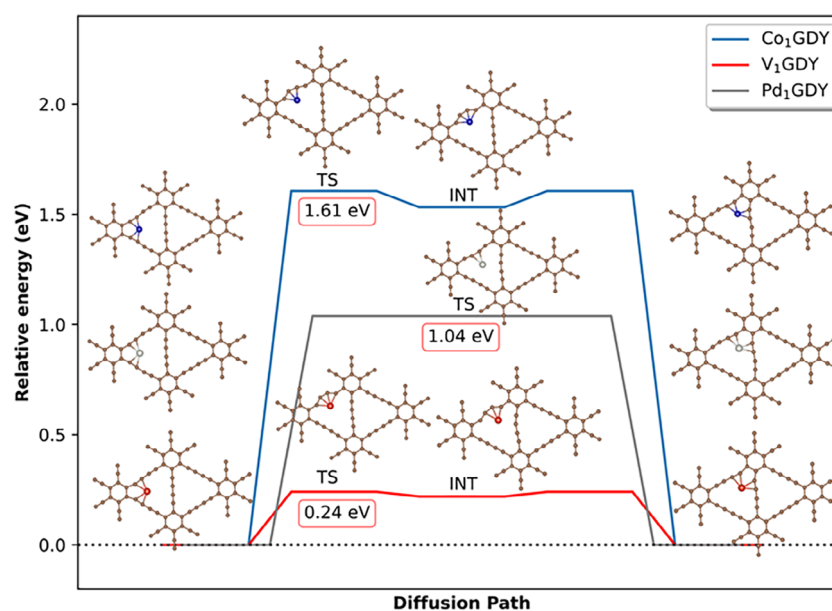


FIGURE 3 | NEB calculation of the relative energies along the diffusion path of a TM atom from its position in a corner of a triangular pore in GDY to an equivalent position in the same pore. Transition states (TS) and intermediate states (INT) are indicated.

investigated (Figure 4). For this purpose, the atom has to cross from one side to the other side of a carbon chain. The final dimer configurations correspond to the ground state structures in 2Co-GDY and 2Pd-GDY. Although the final configurations are more stable than the initial ones in these two cases, there are high energy barriers, of 1.99 and 0.94 eV for Co and Pd, respectively, along the corresponding diffusion paths. Unlike Co and Pd, the final V_2 configuration is less stable than the adsorption of two individual V atoms in two different pores, and a high energy barrier of 1.99 eV is found in the path to dimerization. Therefore, diffusion of V, Co, and Pd atoms across the GDY surface leading to aggregation of atoms is unlikely at moderate temperatures, because of the presence of high barriers.

Li et al. [37] have emphasized the necessity of a large atom-support interaction to guarantee the stability of SACs. Our work shows that dispersion of individual V, Co, or Pd atoms on GDY leads to stable structures, because high adsorption energies and large diffusion barriers prevent atom aggregation at ambient conditions and, therefore, are good candidates for SACs. This conclusion supports experimental observations of TM-SACs on GDY substrates. Zhou et al. [38] synthesized SACs formed by Co, Rh, and Ru atoms on GDY. These were investigated for the production of NH_3 from nitrogen and water, and Rh was particularly effective. Lu and Wang [39] review work on the synthesis of SACs of Fe, Ni, Co, Cu, Ru, Rh, and Pd on GDY, and their applications in hydrogen and oxygen evolution reactions, and oxygen, nitrogen, and CO_2 reduction reactions. Yu and coworkers [40] introduced a method to synthesize Cu-GDY SACs. The single-atom structure was confirmed by using synchrotron radiation and several spectroscopies, and high activity in the direct benzene oxidation to phenol was found. Zhang et al. [41] built Ru-SACs anchored on nitrogen-doped GDY quantum dots, which were successful in the selective hydro-dehalogenation and hydro-dearomatization of chlorophenols.

An advantage of GDY in comparison with related supports for SACs, such as graphene, is that the adsorption energies of TM atoms on GDY are large (see Table 1), while the adsorption energies on graphene are substantially smaller [42]. Taking Pd as an example, E_a values are 2.65 eV on GDY, and 1.08 eV on graphene. Diffusion barriers of Pd on graphene are small [30]. A Pd atom can easily move on the graphene surface through a highway formed by the network of sides of the hexagons, finding barriers of only 0.06 eV, while the barriers in GDY are an order on magnitude larger. This problem can be solved in graphene by creating vacancies, which bind tightly the metal atoms via the dangling bonds [43, 44], but this is not necessary in GDY.

2.3 | Adsorption of Transition Metal Atoms on BGDY

In a previous study [45], we investigated the adsorption of V, Co, and Pd atoms, and V_6 , Co_6 , and Pd_6 clusters on BGDY. In contrast with the present study, in that work the calculations were performed with fixed values of the cell parameters of the BGDY lattice; that is, relaxation of the dimensions and shape of the cell upon adsorption of metal atoms and clusters were not allowed. A fixed cell is well suited to represent a low concentration of metal dopants (one atom or cluster adsorbed per several -four or more- unit cells), since in that case a very small global relaxation, or even no relaxation of the cell of the supporting layer is expected. That is, the effect of the metal dopant is to induce just a local deformation of the structure of the BGDY carbon chains without affecting the overall lattice shape and size. This is shown in Figure S4. However, larger doping, with one or more metal atoms or one cluster per unit cell, might induce substantial changes in the cell size and shape. To address this issue, calculations were performed allowing for relaxation of the size and

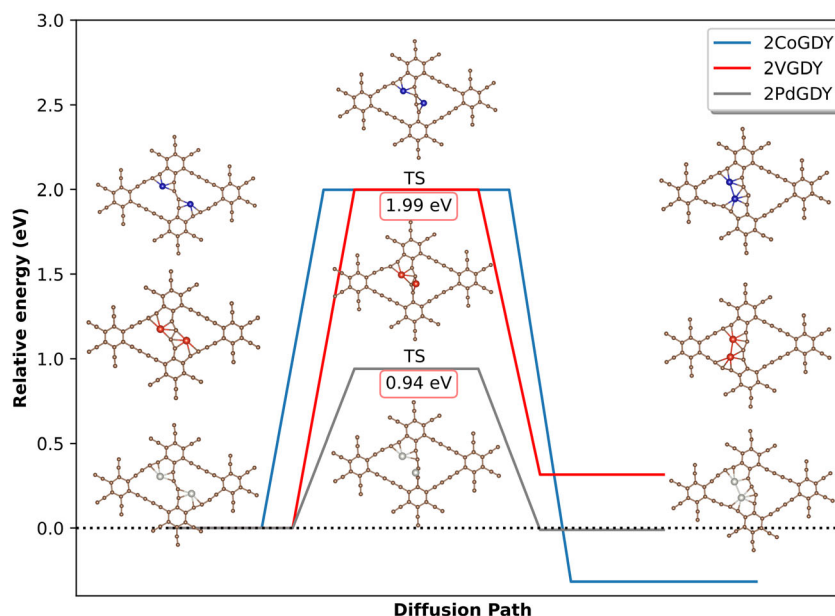


FIGURE 4 | NEB calculation of the relative energies along the diffusion path of a TM atom from one pore of GDY to an adjacent pore already occupied by other TM atom, crossing from one side to the other side of a carbon chain. Transition states (TS) are indicated. For Co and Pd, the dimer configuration (final state) is the ground state structure.

shape of the cell, in addition to relaxation of the positions of all the atoms in the cell, for each nTM-BGDY system.

The adsorption of V, Co, or Pd atoms on BGDY occurs preferentially at the C-B-C corners of the hexagonal holes, sitting out of plane and linked to the two carbon chains that form the corner (Figure 5). Adsorption of one V atom per unit cell induces the deformation of the BGDY cell, with a substantial change of the cell parameters: enlarging a by 6.7%, shortening b by 8.4%, and reducing the angle γ by 3.7%. For Co, the corresponding changes are 5.9%, 8.4%, and 3.4%. Pd leads to negligible cell relaxation.

The adsorption energies of V, 3.70 eV, and Co, 3.41 eV (Table 3) are 10.8% and 11.8%, respectively, higher than the corresponding adsorption energies on the fixed BGDY cell [45]. Clearly, cell relaxation allows for a better accommodation of the metal dopants. This increases the strength of the metal-carbon bonding which compensates the energy of the layer distortion, leading to a higher stability of the doped layer. On the other hand, the adsorption energy of Pd, 2.40 eV, is nearly the same as in

TABLE 3 | Adsorption energies (in eV) and interatomic distances (in Å) of one transition metal atom adsorbed on BGDY. Energies were calculated as in (Equation 1).

System	E_{ads}	d (TM-C)
V-BGDY	3.70	2.10–2.19
Co-BGDY	3.41	1.89–2.02
Pd-BGDY	2.40	2.15–2.72

the fixed BGDY cell, because there is no cell relaxation. Interestingly, V and Co atoms have substantially higher adsorption energies than Pd on both GDY and BGDY layers. V and Co are elements of the 3d period with unfilled d shells (having electronic configurations $3d^3 4s^2$, and $3d^7 4s^2$, respectively) and their interaction with the carbon substrates is strong. Pd is an element with the 4d shell filled, which leads to a weaker interaction.

Decoration of BGDY with a second TM atom on a different corner of the hole can be done in three different nonequivalent configurations shown in Figure S5. After relaxation, the lowest

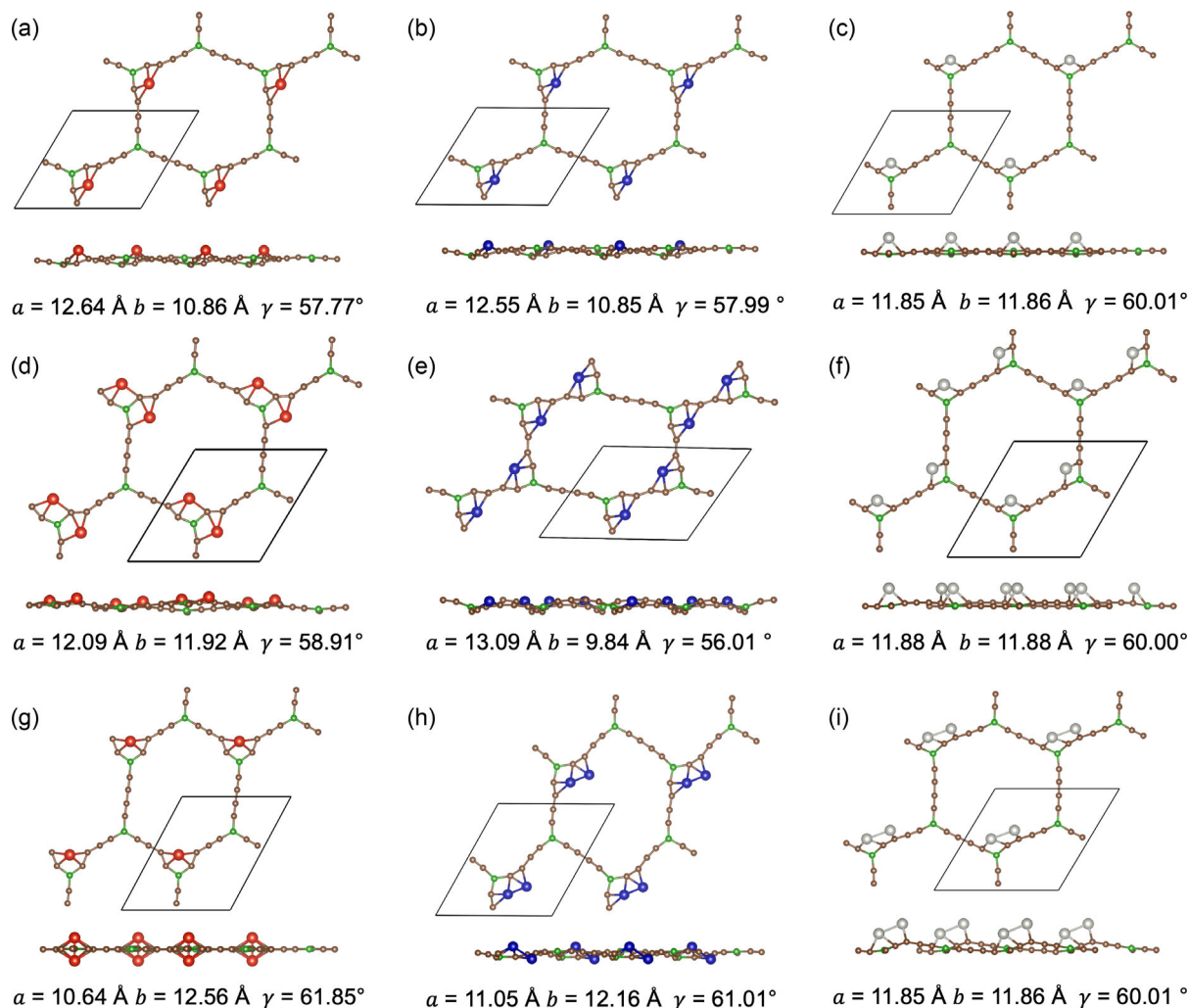


FIGURE 5 | Upper panel: Front and side views of BGDY with one adsorbed TM atom per unit cell; (a) V, (b) Co, and (c) Pd. Vanadium is shown in red, cobalt in blue, and palladium in gray color. For better visualization, the unit cell is repeated four times. In all cases, the a , b , and γ parameters of the optimized cells are indicated. Middle panel: Similar plots for two TM atoms decorating BGDY in different corners: (d) 2V, (e) 2Co and (f) 2Pd. Lower panel: Lowest energy configuration of two V (g), two Co (h), and two Pd atoms (i) allowed to form V_2 , Co_2 and Pd_2 clusters.

energy configurations for two V, two Co, and two Pd atoms are shown in Figure 5. In the case of V, the three configurations compete in energy (Table S4), with an energy difference among them lower than 0.13 eV. In the most stable structure, the two V atoms are adsorbed on two corners sharing the B atom, the V–V distance is 3.87 Å, and therefore there is not direct bond between the two atoms (the bond length of free V_2 is 1.77 Å) [31, 32]. The adsorption energy of the second V atom, 2.70 eV, is substantially smaller (1 eV lower) than that of the first V atom (compare Tables 3 and S4), because in the case of two adsorbed V atoms, each V atom forms bonds with three C atoms, while for adsorption of a single V atom, this atom forms bonds with four C atoms. Decoration of BGDY with two Pd atoms does not deform the BGDY cell and the three configurations for the two adsorbed atoms have the same energy (Table S4). The adsorption energies of the first and second Pd atoms are similar, only 0.06 eV smaller for the second atom (compare Tables 3 and S4). Unlike Pd and V, adsorption of a second Co atom induces additional deformations of the shape of the BGDY cell. The hexagonal hole shrinks in the direction of one apothem, enlarging a , and shortening b and γ . The planarity of the substrate is also affected. The second Co atom was adsorbed with a slightly smaller energy than the first one (3.31 and 3.41 eV, respectively).

Other configurations with two adsorbed atoms per cell, different from those in Figure S5, have also been investigated. Specifically, the second atom was allowed to occupy the same corner as the first one to form a dimer. In this way, a V_2 cluster perpendicular to the BGDY layer, whose optimized structure is shown in Figure 5g, is more stable than the configuration of Figure 5d. One V atom of the cluster is above, and the other below the layer plane, and the V–V distance is 2.15 Å. The adsorption energy of the second V atom, taking as reference the structure with one adsorbed V atom in Figure 5a, is 4.02 eV; this value is 1.32 eV higher, compared to the case of decoration of the layer (Figure 5d), and this can be ascribed to V–V bonding. For palladium, the structure with one Pd_2 cluster is shown in Figure 5i. This structure is a bit more stable than the decoration structures of Figure S5 (compare the adsorption energies of the second Pd atom in Tables 4 and S4). The distance between the two Pd atoms in the adsorbed Pd_2 cluster is 2.61 Å. In contrast with V and Pd, formation of a Co_2 cluster on BGDY (Figure 5h) is less stable (0.81 eV lower) than the decoration of the surface with two Co atoms in different corners. In conclusion, after comparing decoration and cluster configurations of two adsorbed TM atoms, the adsorption energy of a second metal atom in its lowest energy configuration is given in Table 4. Similar to the adsorption of the first metal atom on the layer, V has the highest adsorption energy

for the second V atom, and Pd has the smallest one among the three studied metals.

Different possibilities for the adsorption of three atoms per cell were investigated, and the results are reported and discussed in Section S5. The most stable structure of three V atoms is the formation of a triangular V_3 cluster, but Co and Pd do not form trimer clusters on the surface of BGDY.

2.4 | Diffusion of TM Atoms on BGDY

V, Co, and Pd atoms have high adsorption energies on BGDY. However, the development of SACs also requires avoiding aggregation of the metal atoms on the supporting surface. To investigate the diffusion of TM atoms, we have performed NEB calculations of the activation barriers. Figure 6 shows the minimum energy paths for diffusion of V, Co, and Pd atoms on the BGDY surface, from an initial position in one C–B–C corner to a neighboring corner in the same pore. The high activation barriers obtained, 1.02 and 1.52 eV for V and Co, respectively, prevent atom diffusion at moderate temperatures. The barrier for Pd is lower, 0.60 eV, and therefore diffusion cannot be discarded.

The activation energy barriers for the crossing of a TM atom from a hexagonal hole to an adjacent hole in order to form a TM_2 cluster have been also investigated (Figure 7). Although the V_2 dimer is more stable (by 1.32 eV) than two individual V atoms adsorbed on adjacent corners of the layer sharing a B atom, a large energy barrier of 0.93 eV would prevent V_2 formation. The barrier for Pd diffusion is small, 0.33 eV, and would not be sufficient to avoid aggregation of Pd atoms. Formation of Co_2 is energetically unfavorable with respect to two separate adsorbed Pd atoms, and in addition a barrier of 1.46 eV for crossing between adjacent holes would make difficult the formation of the dimer. In summary starting from well-dispersed metal atoms on BGDY, large enough energy barriers prevent aggregation of atoms in the case of V and Co, giving support to the stability of SAC platforms of V and Co on BGDY. The moderate barriers found for Pd, however, may compromise the development of Pd SACs. Since experiments investigating BGDY as a support for SACs have not been performed, this work may motivate that research.

2.5 | Discussion of the Interaction Between TM Atoms and GDY and BGDY Supports

V, Co, and Pd are adsorbed on both GDY and BGDY layers with high adsorption energies. However, significant differences appear between the two supporting layers, and also among the three metals. Negligible distortions (smaller than 0.5%) of the lattice parameters and angle γ occur upon adsorption of V, Co, and Pd (one, two or three atoms) on GDY, although local distortions of the carbon chains are observed. In contrast, sizable distortions of BGDY take place upon adsorption of V and Co (one, two or three atoms), but the distortions are negligible for Pd. That is, adsorption of these metals behaves differently depending on the support. This can be explained because BGDY pores are larger than GDY pores, 13.72 and 6.94 Å respectively (see Figure 1), and furthermore, the carbon chains are linked to hexagonal benzoic cycles in GDY. This makes the

TABLE 4 | Adsorption energies of a second TM atom on BGDY with one preadsorbed TM atom. Energies are given in eV and interatomic distances in Å. The preferred structures are formation of V_2 and Pd_2 clusters, and decoration with two Co atoms.

System	E_{ads} (eV)	d (TM–C)	d (TM–TM)
V_2 -BGDY	4.02	1.97–2.06	2.15
2Co-BGDY	3.31	1.89–2.00	5.06
Pd_2 -BGDY	2.44	1.99–2.19	2.61

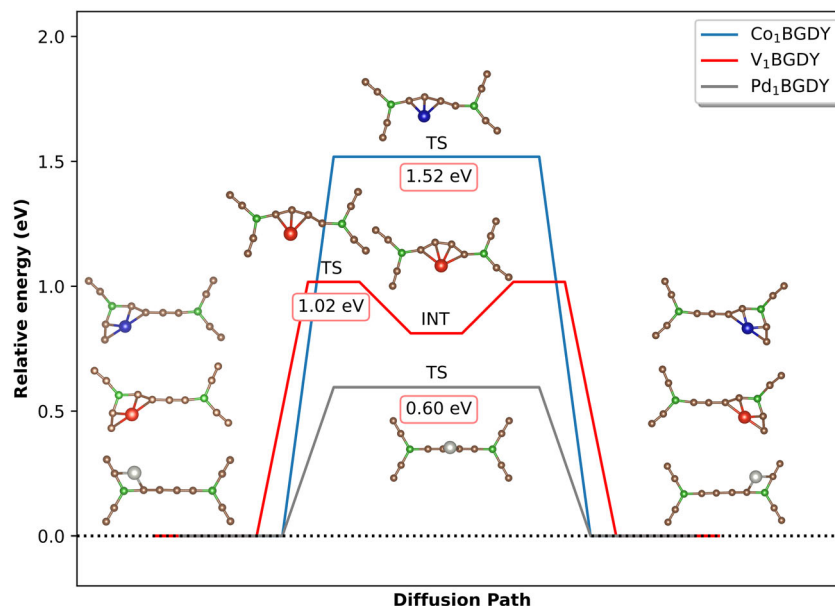


FIGURE 6 | NEB calculation of the relative energies along the diffusion path of V, Co, and Pd atoms parallel to a carbon chain from its ground state configuration on a C-B-C corner of BGDY to a neighboring corner. V is in red, Co in blue, and Pd in gray color. Transition states (TS), intermediate states (INT), and values of the activation barriers are indicated.

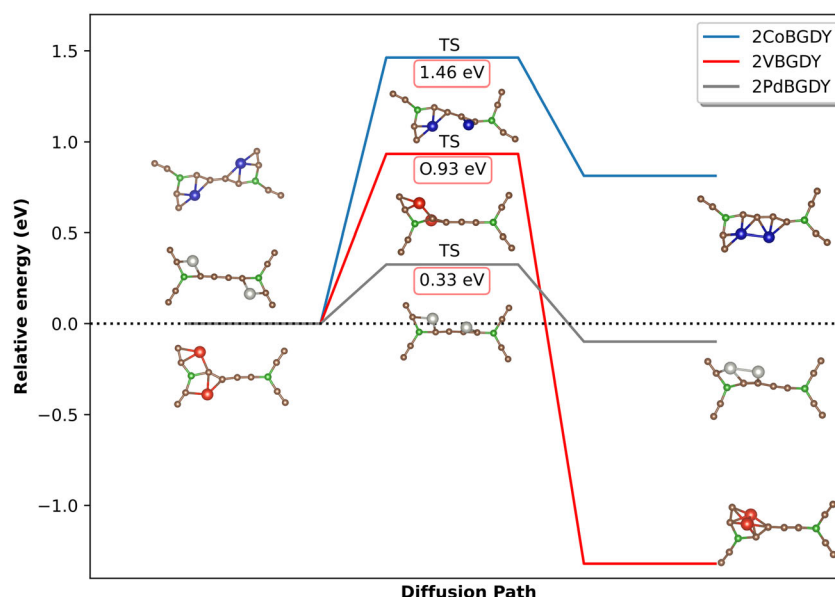


FIGURE 7 | NEB calculation of the minimum energy path for the formation of a TM_2 cluster starting from atoms in neighbor hexagonal holes. Transition states (TS) are shown.

structure of GDY more rigid, while the deformations caused by metal–support interaction become more pronounced in BGDY. On the other hand, the adsorption energies are higher for V and Co than for Pd in both substrates. This can be understood because the electronegativity of Pd is higher than those of Co and V (2.20, 1.88, and 1.63, respectively, in the Pauling scale (see also ref. [46]), indicating that V and Co can transfer electrons to the substrate more easily than Pd.

To get additional information on the TM-BGDY support interaction, Figure 8 shows the electron density redistribution upon adsorption of one V, Co, or Pd atom on BGDY. The substantial

density redistribution around the TM atom and the neighboring carbon chains reflects the strong interaction of these atoms with the support. For V and Co, the electron redistribution is more recognizable compared to Pd, in agreement with the magnitude of the adsorption energies. Regions of enhanced electron density are mainly located on the substrate chains and are larger for adsorption of V and Co, as expected from the electronegativities. Atomic charges have been calculated using a Voronoi cell partition of space. The results for clean GDY and BGDY layers and for layers with one adsorbed TM atom are given in Table S7 and discussed in Section S6. The TM atoms lose electronic charge, and the charge transferred to the substrate is larger

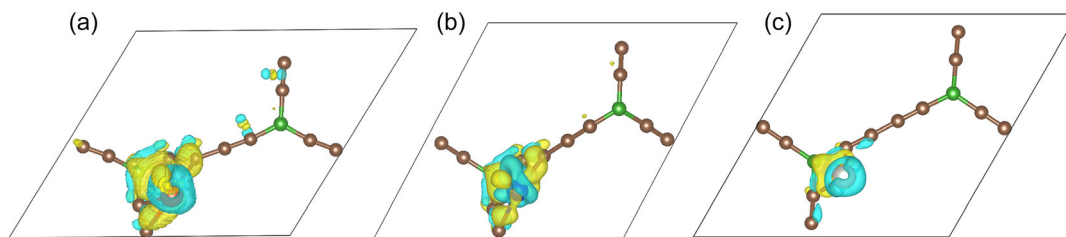


FIGURE 8 | Electron density redistribution upon adsorption of V (a), Co (b), or Pd (c) atoms on BGDY. Yellow and blue colors indicate regions of increase and decrease of electron density, respectively. Isosurface values were set to $\pm 0.0065 \text{ e}/\text{\AA}^3$.

for V, as compared to Co and Pd. A sizable part of this charge goes to the B atoms in BGDY, and the rest is shared between the C atoms. All the charge is shared between C atoms in GDY.

Tables 1 and 3 show metal–carbon bond lengths, $d(\text{TM}-\text{C})$, for adsorption of a metal atom on GDY and BGDY, respectively. These bond lengths are larger for adsorption on BGDY, because BGDY holes are larger than GDY holes, and the angles at the corners of the BGDY hexagons are more open than those in the GDY triangles, constraining less the adsorbed atoms. In an experimental situation characterized by low metal atom coverage, aggregation of atoms requires a number of diffusion steps of two types: a) diffusion from an initial location to another in the same hole (typically, from one corner to another); b) diffusion of the atom from a hole to an adjacent hole. In GDY, those two steps correspond to Figures 3 and 4, respectively. All activation barriers are large for V and Co. For Pd, although the barrier in Figure 3 is low, the barrier in Figure 4 is high. Consequently, long range diffusion through GDY will be difficult for V, Co, and Pd atoms, and formation of stable SACs can be expected in the three cases. For a BGDY substrate, barriers for diffusion in the same hole (Figure 6) are large for V and Co, while Pd is at the limit. Barriers to cross from one pore to a neighbor one are again large for V and Co and small for Pd (see Figure 7). This means that V and Co can be used to build SACs on BGDY, but less likely Pd.

2.6 | Adsorption of TM_6 Clusters on GDY and BGDY

In addition to SAC, there is also great interest in the design and development of single cluster catalysts (SCC). Li et al. [47] have reviewed the applicability and great potential of SCC. Small TM clusters of selected sizes dispersed on suitable supports may serve to build stable and efficient SCCs. We investigated the adsorption of V_6 , Co_6 , and Pd_6 clusters on GDY and BGDY. The free clusters, shown in the insets of Figure 9, have octahedral configurations, a bit distorted in V_6 [45]. Those clusters have relatively large cohesive energies, 2.61, 2.94, and 1.97 eV per atom for V_6 , Co_6 , and Pd_6 , respectively [45].

Several adsorption positions and orientations of TM_6 clusters on GDY (above a hexagon and above a triangular pore) and BGDY (above a B atom, at a C-B-C corner and next to a C chain) were studied. TM_6 clusters are preferentially adsorbed on the triangular holes of GDY, causing local deformations of the carbon chains bounding the triangle, but negligible global distortion of the lattice (see Figure 9). The octahedral structure of the clusters is preserved, with little deformation. In the most stable configuration

of adsorbed V_6 , the lowest apex atom crossed the triangular hole to the other side of the layer. The equatorial rectangle of the cluster is tilted by 20° with respect to the layer plane, with two opposed V atoms of that rectangle located at two corners or the hole (one in plane and one out of plane). The other two equatorial atoms are slightly out of the GDY plane, one sitting at the third corner of the triangular pore and the other near the center of the carbon chain opposite to that corner. The V–C bond lengths vary between 1.99 and 2.27 \AA , values consistent with those observed in the adsorption of one, two, and three V atoms. The upper-apex V atom is not bound to the C atoms of the substrate. Co_6 is adsorbed in such a way that one on the triangular faces of the octahedron is on the layer plane, each atom of that face placed near a corner of the triangular hole. The three Co atoms of the parallel face sit 2.3 \AA above the GDY layer. All Co atoms of the cluster form bonds with atoms of the carbon chains. The Co–Co bond lengths are 2.30 \AA for the upper atoms, and 2.55 \AA for the base atoms, revealing some distortion of the octahedron. One triangular face of Pd_6 is placed a little above the GDY layer and tilted with respect to the layer, in this way allowing one Pd atom of the upper face to form bonds with carbon atoms. Due to the presence of the cluster, the neighbor carbon atoms protrude upwards from the layer plane. A view for a repeated cell is shown in Figure S9.

The adsorption energy of TM_6 clusters on GDY (an analogous formula holds for BGDY) is given by:

$$E_{\text{ads}}(\text{TM}_6\text{-GDY}) = E(\text{GDY}) + E(\text{TM}_6) - E(\text{TM}_6\text{-GDY}) \quad (4)$$

where $E(\text{TM}_6)$ and $E(\text{TM}_6\text{-GDY})$ are the energies of the isolated cluster and the cluster adsorbed on GDY, respectively. Adsorption energies of V_6 , Co_6 , and Pd_6 , given in Table 5, are large, confirming the stability of these cluster-GDY platforms.

Adsorption of V_6 and Co_6 induces significant changes in the BGDY lattice, but lattice distortions are less pronounced upon adsorption of Pd_6 (Figure 10). The changes in the lattice parameters a , b , and γ of BGDY are, respectively, -8% , $+4\%$, $+2.9\%$ upon adsorption of V_6 ; -7.3% , -2.8% , $+3.3\%$ upon adsorption of Co_6 ; and -4.7% , -0.1% , 2.0% upon adsorption of Pd_6 . V_6 sits at a corner of a hexagonal hole, linked to two carbon chains, and maintains (slightly deformed) its octahedral structure. A plane containing four V atoms is perpendicular to the BGDY layer, with two V atoms above and two below the layer; two of those V atoms do not form bonds with C atoms. The fifth and sixth atoms of the octahedron are in the layer plane. The carbon chains in contact with V_6 are distorted to optimally accommodate the cluster, but the layer remains planar. Adsorbed Co_6 and Pd_6 change their

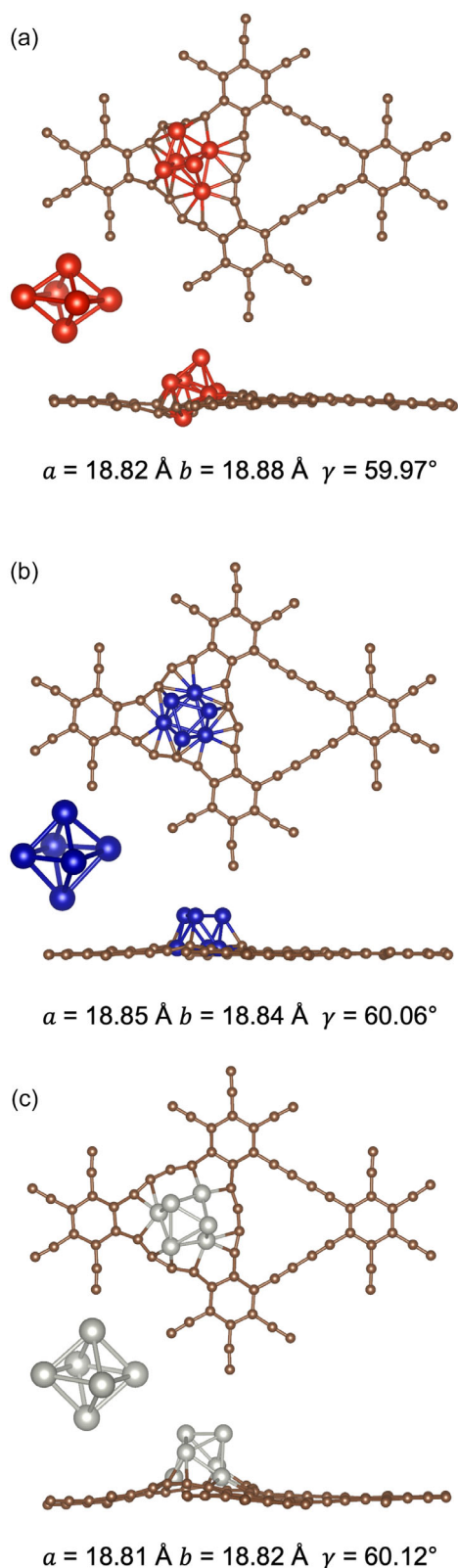


FIGURE 9 | TM_6 clusters adsorbed on GDY. Cell parameters (a , b , and γ) are indicated. Insets show the structures of the free clusters. (a–c) panels stand for V, Co, and Pd, respectively.

structure, adopting a capped triangular bipyramid configuration linked to three carbon chains of a hexagonal hole. The carbon chains bend to enhance the bonding with the clusters. In Co_6 , two Co atoms are above the BGDY layer (at 1.17 and 1.67 Å),

TABLE 5 | Adsorption energies (in eV) of TM_6 clusters on GDY and BGDY.

Cluster	E_{ads} on GDY	E_{ads} on BGDY
V_6	9.31	6.62
Co_6	6.56	4.45
Pd_6	4.55	4.43

three are in plane, and one Co atom crosses to the other side of the layer (at -1.04 Å); the Co–Co bond lengths are between 2.22 and 2.36 Å, and the BGDY layer remains almost planar. All atoms of Pd_6 lie on the same side of the layer, only four of them bonded to carbon atoms.

The TM_6 -BGDY structures described above have been calculated by allowing full relaxation of the BGDY lattice (a , b , and γ) in the limit of high coverage, i.e., one cluster per unit cell. Comparison with the configurations of TM_6 -BGDY obtained without relaxation of the lattice [45], which are adequate to represent low coverage levels, shows the effect of the amount of coverage on the final configurations. Pd_6 induces a small change in the BGDY lattice, and almost identical configurations for the adsorbed cluster are obtained with and without relaxation of the lattice. This indicates that the structure of the substrate is not too sensitive to coverage level in the case of Pd clusters. Larger lattice deformations occur for V_6 and Co_6 . The structure of V_6 is quite similar to that in the unrelaxed lattice. In contrast, the structure of Co_6 is different in the unrelaxed lattice, where Co_6 maintains the octahedral structure and sits above a B atom with a triangular face parallel to the layer. Lattice relaxation leads to the deformation of the hexagonal holes, in a way that favors the interaction of three carbon chains with the embedded Co_6 . The cluster changes its shape to form a capped triangular bipyramid to enhance its interaction with BGDY. Thus, different catalytic activities might be expected for Co_6 SCCs depending on the level of cluster coverage of the layer. In conclusion, the adsorption energies of V_6 , Co_6 , and Pd_6 on GDY and BGDY (Table 5) are quite high. In fact, for Pd_6 , those adsorption energies are several times larger than the adsorption energies of Pd_6 and other Pd_n clusters of similar size on graphene [30]. This highlights the enhanced stability and gives support to the proposal of building SCCs based on V_6 , Co_6 , and Pd_6 clusters adsorbed on GDY and BGDY.

Lu and Wang [39] have reviewed the application to electrocatalysis of clusters and nanoparticles anchored on GDY. Those clusters and nanoparticles are large, in general, but some examples can be selected from the scientific literature on catalytic applications of relatively small clusters adsorbed on GDY. Those clusters are larger than the six-atom clusters we have studied, but our conclusion of the high stability of the six-atom clusters supports the stability of the cluster-GDY systems synthesized in the experiments. By redox reaction between GDY and PdCl_4 , Qi and coworkers [48] synthesized Pd nanoparticles well dispersed on the surface of GDY. Furthermore, using GDY oxide, smaller Pd nanoparticles, of 1.3 nm, were deposited and found to exhibit an excellent catalytic performance for the reduction of 4-nitrophenol with sodium borohydride. Rong et al. [49] prepared Cu catalysts of varying size, from SACs to medium size clusters (0.5–1 nm) to nanoclusters (1–1.5 nm), deposited on

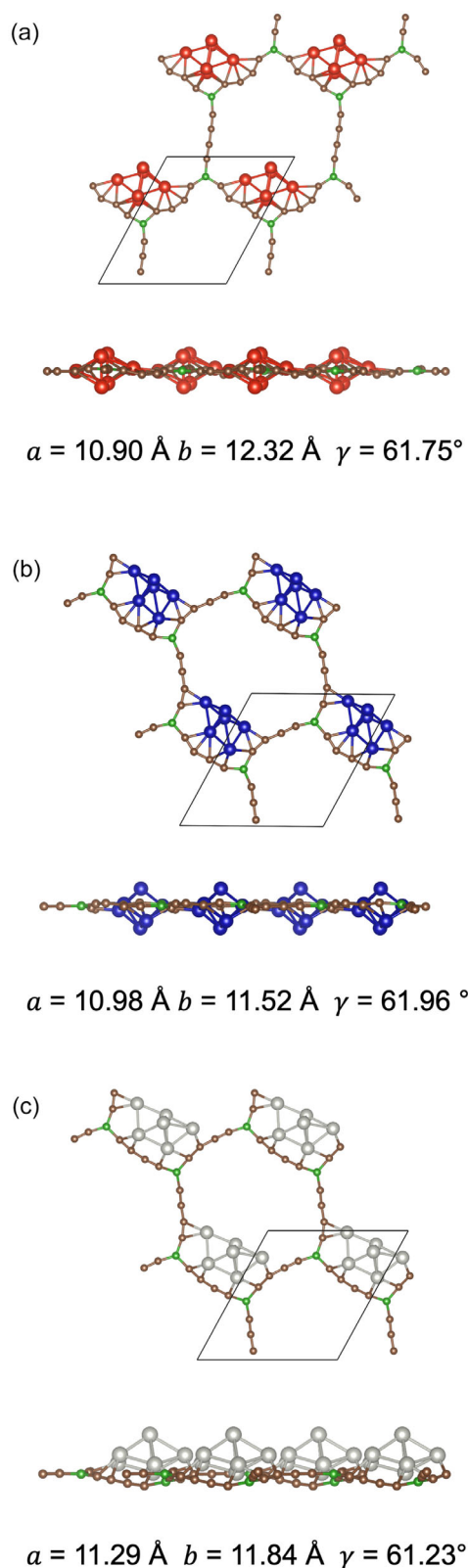


FIGURE 10 | TM_6 clusters adsorbed on a BGDY layer. (a) V_6 -BGDY, (b) Co_6 -BGDY, and (c) Pd_6 -BGDY. Optimized cell parameters are indicated.

GDY. These authors performed electrocatalytic measurements and found a remarkable size dependence of the activity and selectivity during CO_2/CO electroreduction. Yan Lv and coworkers [50] wrapped thick carbon nanotubes with GDY film and the composite was utilized to support Pt clusters on the surface using

an electrochemical reaction method. The average diameter of the Pt clusters was 0.63 nm, and the system exhibited good stability and excellent electrocatalytic activity for the hydrogen evolution reaction.

Finally, densities of electronic states (DOS) of GDY and BGDY with TM atoms and clusters adsorbed are shown in Figures S10–S13. Clean GDY and BGDY have semiconducting character. The adsorption of V and Co atoms on GDY introduces metal states, hybridized with the electronic states of the substrate, and a shift between the energies of the spin up and spin down metal states is evident. Some of the metal states lie in the gap (Figure S10). Adsorption of V and Co on BGDY also displays a shift between spin up and down metal states, but the influence on the gap is less (Figure S11). After adsorption of V_6 , Co_6 , and Pd_6 (Figures S12 and S13), the metal states dominate the DOS near the Fermi energy and the electronic gap is closed, but the shift between spin up and down states is only important for Co, as a reminder of the magnetism of bulk cobalt.

3 | Conclusion

With the aim of gaining insight and contributing to the rational design of single-atom catalysts, and single-cluster catalysts, we have investigated the structure and stability of TM atoms and TM_6 clusters (TM = V, Co, and Pd) supported on GDY and BGDY, by performing density functional calculations. The interaction between the metals and the support is strong, favoring the stability of these systems. The presence of high activation barriers against metal atom diffusion through the support (except for diffusion of Pd on BGDY) prevents the formation of dimers and larger clusters from initially well-separated atoms, this being promissory for the stability and efficiency of SACs. Adsorbed trimer configurations are more stable than the decoration of the layers with isolated atoms, except for Co and Pd on BGDY. However, the formation of those trimers from isolated adsorbed atoms is unlikely due to the high diffusion barriers.

In the case of SCC, clusters of six metal atoms were investigated. The interaction of the clusters with the support is strong, with high adsorption energies on both GDY and BGDY. Adsorption energies are larger on GDY, as compared to BGDY, because the pore holes are smaller in GDY. V_6 was adsorbed on both substrates maintaining its octahedral shape. But Pd_6 , and also Co_6 , interact differently with GDY and BGDY. In BGDY, the clusters lose their octahedral shape while in GDY the adsorption occurs without deformation of the cluster shape. Co_6 and V_6 show the most notable differences in adsorption energies depending on the substrate, differing by 2.11 eV for cobalt and 2.69 eV for vanadium. In summary, deposition of transition metal atoms (V, Co, Pd) and transition metal clusters on GDY and BGDY is a promising way of building stable single atom and single cluster catalysts, respectively.

4 | Experimental Section/Theoretical Model

Adsorption of transition metal (V, Co, and Pd) atoms and clusters on GDY and BGDY layers has been investigated using the DFT formalism. The calculations were performed with the quantum

ESPRESSO package [51, 52], using the Perdew–Burke–Ernzerhof (PBE) functional [53] and the Projected-Augmented-Wave (PAW) pseudopotentials [54, 55]: C.pbe-nkjpaw_psl.1.0.0.UPF for carbon, B.pbe-n-kjpaw_psl.1.0.0.UPF for boron, V.pbe-spnkjpaw_psl.1.0.0.UPF for vanadium, Co.pbe-spn-kjpaw_psl.0.3.1.UPF for cobalt, and Pd.pbe-n-kjpaw_psl.1.0.0.UPF for palladium [56]. With these pseudopotentials, the number of electrons per atom included in the calculations is 4 electrons for carbon, 3 for boron, 13 for vanadium, 17 for cobalt, and 10 for palladium. Plane wave basis sets are used to expand the electronic wave functions and the electronic density. The energy cutoff for the expansion of the electronic wave functions was set to 45 Ry for the adsorption of V and Pd on GDY and BGDY, and to 60 Ry for the adsorption of Co. The energy cutoff for the expansion of the electronic density was set to 360 Ry for V_n-GDY and Pd_n-GDY, 350 Ry for V_n-BGDY and Pd_n-BGDY, and 480 Ry for Co_n-GDY and Co_n-BGDY. All calculations are performed using a 3 × 3 × 1 Monkhorst–Pack k-point sampling [57] in the first Brillouin zone of the reciprocal lattice and were carried out in spin polarized mode. In addition, nudged elastic band (NEB) calculations [36] were performed to study the diffusion barriers of the metal atoms. Atomic charges provide some insight on the metal–support interaction and have been calculated [58] using a Voronoi cell partition scheme.

Author Contributions

Johanna Sandoval Menjivar: conceptualization (equal), formal analysis (equal), investigation (equal), methodology (equal), visualization (lead), writing – original draft (equal). **Estefanía Germán:** conceptualization (equal), formal analysis (equal), funding acquisition (equal), investigation (equal), methodology (equal), supervision (equal), writing – review and editing (equal). **Julio A. Alonso:** conceptualization (equal), formal analysis (equal), investigation (equal), methodology (equal), writing – original draft (equal), writing – review and editing (equal). **Maria J. López:** conceptualization (equal), formal analysis (equal), funding acquisition (lead), investigation (equal), methodology (equal), supervision (equal), validation (equal), writing – review and editing (equal).

Acknowledgments

Work supported by grant PID2022-138340OB-I00 funded by MCIN/AEI/10.13039/501100011033 and FSE+, Junta de Castilla y León (Apoyo a GIR, Project VA029G24), and University of Valladolid (GIR Nanostructure Physics). The authors thankfully acknowledge RES resources provided by i) BSC in MareNostrum 5 to FI-2024-2-0031 and ii) CSUC in Pirineus III to FI-2025-1-0029 and to FI-2025-2-0004. Work by J.S.M. was (partially) supported by the Schlumberger Foundation Faculty for the Future program. J.A.A. acknowledges the hospitality of DIPC.

Funding

This work was supported by MCIN/AEI/10.13039/501100011033 and FSE+ (PID2022-138340OB-I00); Junta de Castilla y León - Apoyo a GIR (VA029G24); University of Valladolid; RES: BSC in MareNostrum 5 (FI-2024-2-0031); RES: CSUC in Pirineus III (FI-2025-1-0029, FI-2025-2-0004); Schlumberger Foundation.

Conflicts of Interest

The authors declare no conflicts of interest.

Data Availability Statement

The data that support the findings of this study are available from the corresponding author upon reasonable request.

References

1. M. Zybert, “Applied Catalysis in Chemical Industry: Synthesis, Catalyst Design, and Evaluation,” *Catalysts* 13 (2023): 607, <https://doi.org/10.3390/catal13030607>.
2. P. M. Ismail, S. Ali, F. Raziq, et al., “Stable and Robust Single Transition Metal Atom Catalyst for CO₂ Reduction Supported on Defective WS₂,” *Applied Surface Science* 624 (2023): 157073, <https://doi.org/10.1016/j.apsusc.2023.157073>.
3. J. Jeskey, Y. Ding, Y. Chen, et al., “Single-Atom Catalysts for Selective Oxygen Reduction: Transition Metals in Uniform Carbon Nanospheres with High Loadings,” *Journal of the American Chemical Society* 3 (2023): 3227–3236, <https://doi.org/10.1021/jacsau.3c00557>.
4. A. Shah, S. Sarfaraz, M. Yar, N. Sheikh, H. Hammud, and K. Ayub, “Remarkable Single Atom Catalyst of Transition Metal (Fe, Co & Ni) Doped on C₂N Surface for Hydrogen Dissociation Reaction,” *Nanomaterials* 13 (2023): 29, <https://doi.org/10.3390/nano13010029>.
5. A. Lasia, “Hydrogen Evolution Reaction,” in *Handbook of Fuel Cells-Fundamentals, Technology and Applications*, Vol. 2, ed. W. Vielstich, H. A. Gasteiger, and A. Lamm (John Wiley & Sons, 2003), 416–440, <https://doi.org/10.1002/9780470974001.f204033>.
6. K. Nose and T. Okabe, “Platinum Group Metals Production,” in *Treatise on Process Metallurgy*, Vol. 3, ed. S. Seetharaman (Elsevier, 2014), 1071–1097, chapter 2.10, <https://doi.org/10.1016/B978-0-08-096988-6.00018-3>.
7. R. Langeslay, D. Kaphan, C. Marshall, P. Stair, A. Sattelberger, and M. Delferro, “Catalytic Applications of Vanadium: A Mechanistic Perspective,” *Chemical Reviews* 119, no. 4 (2019): 2128–2191, <https://doi.org/10.1021/acs.chemrev.8b00245>.
8. C. Bauer, F. Müller, S. Keskin, M. Zobel, and R. Kempe, “A Highly Active Cobalt Catalyst for the General and Selective Hydrogenation of Aromatic Heterocycles,” *Chemistry - A European Journal* 29 (2023): e202300561, <https://doi.org/10.1002/chem.202300561>.
9. J. Gao, C. Ren, X. Huo, et al., “Supported Palladium Catalysts: A Facile Preparation Method and Implications to Reductive Catalysis Technology for Water Treatment,” *ACS ES&T Engineering* 1 (2021): 562–570, <https://doi.org/10.1021/acsestengg.0c00227>.
10. J. Wan, C. Wang, Q. Tang, X. Gu, and M. He, “First-Principles Study of Vanadium Carbides as Electrocatalysts for Hydrogen and Oxygen Evolution Reactions,” *RSC Advances* 9 (2019): 37467–37473, <https://doi.org/10.1039/C9RA06539C>.
11. S. Gupta, R. Fernandes, R. Patel, M. Spreitzer, and N. Patel, “A Review of Cobalt-Based Catalysts for Sustainable Energy and Environmental Applications,” *Applied Catalysis A: General* 661 (2023): 119254, <https://doi.org/10.1016/j.apcata.2023.119254>.
12. L. Zhang, Q. Chang, H. Chen, and M. Shao, “Recent Advances in Palladium-Based Electrocatalysts for Fuel Cell Reactions and Hydrogen Evolution Reaction,” *Nano Energy* 29 (2016): 198–219, <https://doi.org/10.1016/j.nanoen.2016.02.044>.
13. B. Ye, B. Jeong, M.-J. Lee, et al., “Recent Trends in Vanadium-Based SCR Catalysts for NO_x Reduction in Industrial Applications: Stationary Sources,” *Nano Convergence* 9 (2022): 51, <https://doi.org/10.1186/s40580-022-00341-7>.
14. K. M. Kaprielova, I. I. Ovchinnikov, O. A. Yakovina, and A. S. Lisitsyn, “Synthesis of Pt/C Catalysts through Reductive Deposition: Ways of Tuning Catalytic Properties,” *ChemCatChem* 5 (2013): 2015–2024, <https://doi.org/10.1002/cctc.201200769>.
15. S. Lu, Y. Zhang, F. Lou, and Z. Yu, “Theoretical Study of Single Transition Metal Atom Catalysts Supported on Two-Dimensional Nb₂NO₂ for Efficient Electrochemical CO₂ Reduction to CH₄,” *Journal of CO₂ Utilization* 62 (2022): 102069, <https://doi.org/10.1016/j.jcou.2022.102069>.
16. G. Busca, “Structural, Surface, and Catalytic Properties of Aluminas,” in *Advances in Catalysis*, Vol. 57, ed. F. C. Jentoft (Academic Press, 2014), Chapter 3, ISSN 0360-0564.

17. A. Shivhare, A. Kumar, and R. Srivastava, "The Size-Dependent Catalytic Performances of Supported Metal Nanoparticles and Single Atoms for the Upgrading of Biomass-Derived 5-Hydroxymethylfurfural, Furfural, and Levulinic Acid," *ChemCatChem* 14 (2022): e202101423, <https://doi.org/10.1002/cctc.202101423>.
18. X. Zhou, W. Xu, G. Liu, D. Panda, and P. Chen, "Size-Dependent Catalytic Activity and Dynamics of Gold Nanoparticles at the Single-Molecule Level," *Journal of the American Chemical Society* 132 (2010): 138–146, <https://doi.org/10.1021/ja904307n>.
19. L. Liu and A. Corma, "Metal Catalysts for Heterogeneous Catalysis: From Single Atoms to Nanoclusters and Nanoparticles," *Chemical Reviews* 118 (2018): 4981–5079, <https://doi.org/10.1021/acs.chemrev.7b00776>.
20. B. Qiao, A. Wang, X. Yang, et al., "Single-Atom Catalysis of CO Oxidation Using Pt₁/FeO_x," *Nature Chemistry* 3 (2011): 634–641, <https://doi.org/10.1038/nchem.1095>.
21. X. Chen, R. Paul, and L. Dai, "Carbon-Based Supercapacitors for Efficient Energy Storage," *National Science Review* 4, no. 3 (2017): 453–489, <https://doi.org/10.1093/nsr/nwx009>.
22. E. Pérez, V. Calvino, and E. Soriano, "Metal-Supported Carbon-Based Materials: Opportunities and Challenges in the Synthesis of Valuable Products," *Catalysis Science & Technology* 6 (2016): 1265–1291, <https://doi.org/10.1039/C5CY01437A>.
23. X. Gao, H. Liu, D. Wang, and J. Zhang, "Graphdiyne: Synthesis, Properties, and Applications," *Chemical Society Reviews* 48, no. 3 (2019): 908–936, <https://doi.org/10.1039/C8CS00773J>.
24. N. Wang, X. Li, Z. Tu, et al., "Synthesis and Electronic Structure of Boron-Graphdiyne with an Sp-Hybridized Carbon Skeleton and Its Application in Sodium Storage," *Angewandte Chemie* 130 (2018): 4032–4037, <https://doi.org/10.1002/ange.201800453>.
25. D. Zhang, X. Li, W. Liu, et al., "Research of Graphdiyne Materials Applied for Electrochemical Energy Storage," *Nano Trends* 4 (2023): 100017, <https://doi.org/10.1016/j.nwnano.2023.100017>.
26. B. Mortazavi, M. Shahrokhi, X. Zhuang, and T. Rabczuk, "Boron-graphdiyne: A Superstretchable Semiconductor with Low Thermal Conductivity and Ultrahigh Capacity for Li, Na and Ca Ion Storage," *Journal of Materials Chemistry A* 6 (2018): 11022–11036, <https://doi.org/10.1039/C8TA02627K>.
27. E. German, J. Sandoval, A. Recio, A. Seif, J. A. Alonso, and M. J. López, "Supported Metal Nanohydrides for Hydrogen Storage," *Chemistry of Materials* 35 (2023): 1134–1147, <https://doi.org/10.1021/acs.chemmater.2c03106>.
28. Y. Abdullahi, M. Rahmana, H. Zainuddina, and S. Abubakar, "First-Principle Study of Geometric Stabilities, Electronic and Magnetic Properties of Low Coverage Vanadium Adsorption on Graphene," *AIP Conference Proceedings* 1588 (2014): 225–229, <https://doi.org/10.1063/1.4866950>.
29. A. N. Rudenko, F. J. Keil, M. I. Katsnelson, and A. I. Lichtenstein, "Adsorption of Cobalt on Graphene: Electron Correlation Effects From a Quantum Chemical Perspective," *Physical Review B* 86 (2012): 075422, <https://doi.org/10.1103/PhysRevB.86.075422>.
30. J. A. Alonso and M. J. López, "Palladium Clusters, Free and Supported on Surfaces, and Their Applications in Hydrogen Storage," *Physical Chemistry Chemical Physics* 24 (2022): 2729–2751, <https://doi.org/10.1039/D1CP03524J>.
31. P. R. R. Langridge-Smith, M. D. Morse, G. P. Hansen, R. E. Smalley, and J. Merer, "The Bond Length and Electronic Structure of V₂," *Journal of Chemical Physics* 80 (1984): 593–600, <https://doi.org/10.1063/1.446769>.
32. E. M. Spain, J. M. Behm, and M. D. Morse, "The 846 nm A' ³Σ_u⁺←X ³Σ_g⁺ Band System of Jet-Cooled V₂," *Journal of Chemical Physics* 96 (1992): 2511–2516, <https://doi.org/10.1063/1.462002>.
33. A. Kant and B. Strauss, "Dissociation Energies of Diatomic Molecules of the Transition Elements. II. Titanium, Chromium, Manganese, and Cobalt," *Journal of Chemical Physics* 41 (1964): 3806–3808, <https://doi.org/10.1063/1.1725817>.
34. B. Kalita and R. C. Deka, "Stability of Small Pd_n (n=1–7) Clusters on the Basis of Structural and Electronic Properties: A Density Functional Approach," *Journal of Chemical Physics* 127 (2007): 244306, <https://doi.org/10.1063/1.2806993>.
35. I. Cabria, M. J. López, and J. A. Alonso, "Theoretical Study of the Transition From Planar to Three-Dimensional Structures of Palladium Clusters Supported on Graphene," *Physical Review B* 81 (2010): 035403, <https://doi.org/10.1103/PhysRevB.81.035403>.
36. G. Henkelman, B. P. Uberuaga, and H. Jónsson, "A Climbing Image Nudged Elastic Band Method for Finding Saddle Points and Minimum Energy Paths," *Journal of Chemical Physics* 113 (2000): 9901–9904, <https://doi.org/10.1063/1.1329672>.
37. J. Li, C. Chen, L. Xu, et al., "Challenges and Perspectives of Single-Atom-Based Catalysts for Electrochemical Reactions," *JACS Au* 3 (2023): 736–755, <https://doi.org/10.1021/jacsau.3c00001>.
38. H. Zou, W. Rong, S. Wei, Y. Jic, and L. Duan, "Regulating Kinetics and Thermodynamics of Electrochemical Nitrogen Reduction with Metal Single-Atom Catalysts in a Pressurized Electrolyser," *Proceedings of the National Academy of Sciences of the United States of America* 117 (2020): 29462–29468, <https://doi.org/10.1073/pnas.2015108117>.
39. T. Lu and H. Wang, "Graphdiyne-Supported Metal Electrocatalysts: From Nanoparticles and Cluster to Single Atoms," *Nano Research* 15 (2022): 9764–9778, <https://doi.org/10.1007/s12274-022-4157-1>.
40. J. Yu, C. Cao, H. Jin, et al., "Uniform Single Atomic Cu₁-C₄ Sites Anchored in Graphdiyne for Hydroxylation of Benzene to Phenol," *National Science Review* 9, no. 9 (2022): nwac018, <https://doi.org/10.1093/nsr/nwac018>.
41. C. Zhang, Y. Li, Y. Xie, et al., "High-Loading Single-Atom Ru Catalysts Anchored on N-Doped Graphdiyne/γ-Graphyne Quantum Dots for Selective Hydrodehalogenation and Hydrodearomatization," *ACS Catalysis* 13 (2023): 12425–12435, <https://doi.org/10.1021/acscatal.3c01390>.
42. J. A. Alonso and M. J. López, "Interaction of Hydrogen with Graphitic Surfaces, Clean and Doped with Metal Clusters," in *Handbook of Materials Modeling*, ed. W. Andreoni and S. Yip (Springer Nature Switzerland, 2020), 545–565, https://doi.org/10.1007/978-3-319-44680-6_32.
43. M. J. López, I. Cabria, and J. A. Alonso, "Palladium Clusters Anchored on Graphene Vacancies and Their Effect on the Reversible Adsorption of Hydrogen," *Journal of Physical Chemistry C* 118 (2014): 5081–5090, <https://doi.org/10.1021/jp410262t>.
44. C. Rivera-Cárcamo and P. Serp, "Single Atom Catalysts on Carbon-Based Materials," *ChemCatChem* 10 (2018): 5058–5091, <https://doi.org/10.1002/cssc.201800453>.
45. J. A. Alonso and L. A. Girifalco, "Electronegativity Scale for Metals," *Physical Review B* 19 (1979): 3889–3895, <https://doi.org/10.1103/PhysRevB.19.3889>.
46. X. Li, S. Mitchell, Y. Fang, et al., "Advances in Heterogeneous Single-Cluster Catalysis," *Nature Reviews Chemistry* 7 (2023): 754–767, <https://doi.org/10.1038/s41570-023-00540-8>.
47. E. German, A. Alvarez-Yenes, J. A. Alonso, and M. A. López, "Adsorption of Transition Metal Clusters on Boron-Graphdiyne," *Applied Surface Science* 548 (2021): 149270, <https://doi.org/10.1016/j.apsusc.2021.149270>.
48. H. Qi, P. Yu, Y. Wang, et al., "Graphdiyne Oxides as Excellent Substrate for Electroless Deposition of Pd Clusters with High Catalytic Activity," *Journal of the American Chemical Society* 137 (2015): 5260–5263, <https://doi.org/10.1021/ja5131337>.
49. W. Rong, H. Zou, W. Zang, et al., "Size-Dependent Activity and Selectivity of Atomic-Level Copper Nanoclusters during CO/CO₂ Electroreduction," *Angewandte Chemie, International Edition* 60 (2021): 466–472, <https://doi.org/10.1002/anie.202011836>.

50. Y. Lv, X. Wu, H. Lin, et al., "A Novel Carbon Support: Few-Layered Graphdiyne- Decorated Carbon Nanotubes Capture Metal Clusters as Effective Metal-Supported Catalysts," *Small* 17 (2021): 2006442, <https://doi.org/10.1002/sml.202006442>.
51. P. Giannozzi, S. Baroni, N. Bonini, et al., "QUANTUM ESPRESSO: A Modular and Open-Source Software Project for Quantum Simulations of Materials," *Journal of Physics: Condensed Matter* 21 (2019): 395502, <https://doi.org/10.1088/0953-8984/21/39/395502>.
52. <https://www.quantum-espresso.org>. (accessed: November, 2025).
53. J. P. Perdew, K. Burke, and M. Ernzerhof, "Generalized Gradient Approximation Made Simple," *Physical Review Letters* 77 (1996): 3865–3868, <https://doi.org/10.1103/PhysRevLett.77.3865>.
54. G. Kresse and D. Joubert, "From Ultrasoft Pseudopotentials to the Projector Augmented Wave Method," *Physical Review B* 59 (1999): 1758–1775, <https://doi.org/10.1103/PhysRevB.59.1758>.
55. P. E. Blöchl, "Projector Augmented-Wave Method," *Physical Review B* 50 (1994): 17953–17979, <https://doi.org/10.1103/PhysRevB.50.17953>.
56. <https://www.quantum-espresso.org/pseudopotentials>. (accessed: November, 2025).
57. H. J. Monkhorst and J. D. Pack, "Special Points for Brillouin-Zone Integrations," *Physical Review B* 13 (1976): 5188–5192, <https://doi.org/10.1103/PhysRevB.13.5188>.
58. <https://theory.cm.utexas.edu/henkelman/code/bader>. (accessed: November, 2025).

Supporting Information

Additional supporting information can be found online in the Supporting Information section. **Supporting Fig. S1:** Different configurations studied for two TM atoms adsorbed on GDY. **Supporting Fig. S2:** Different configurations studied for three TM atoms on GDY. **Supporting Fig. S3:** Lowest energy configurations of three TM atoms adsorbed on GDY. (a) V, (b) Co, (c) Pd. The a , b and γ parameters of the optimized cells are indicated. **Supporting Fig. S4:** Front and side views of the calculated structure of a Co atom adsorbed on BGDY. A large 2×2 cell was used in the calculations to simulate low dopant coverage. The dimensions and shape of the cell were allowed to vary to optimize the energy. The global structure is almost unaltered, and only a local deformation of the BGDY structure is observed near the adsorbed Co atom. For a fixed-cell calculation the cell parameters are: $a = b = 23.70 \text{ \AA}$, $\gamma = 60^\circ$. The Co atom is shown in blue, B in green and C in brown color. **Supporting Fig. S5:** Different configurations studied for two TM atoms adsorbed on BGDY. **Supporting Fig. S6:** Different configurations studied for adsorption of three TM atoms per cell on BGDY. **Supporting Fig. S7:** Top and side views of the most stable structures of three TM atoms on BGDY, per unit cell. (a) V_3 -BGDY, (b) $3Co$ -BGDY, and (c) $3Pd$ -BGDY. **Supporting Fig. S8:** Enumerations of atoms in: (a) TM-GDY and (b) TM-BGDY. Carbon atoms are colored in brown, boron in green and the adsorbed metal atom (V, Co, and Pd) in purple. **Supporting Fig. S9:** Top and lateral views of Pd_6 clusters adsorbed on GDY. The unit cell is repeated in the two directions. **Supporting Fig. S10:** Density of electronic states (DOS) of (a) GDY, (b) V-GDY, (c) Co-GDY, and (d) Pd-GDY, separated in spin-up (black color) and spin-down (red color) states. Blue and green regions correspond to the DOS projected on the TM atoms. **Supporting Fig. S11:** Density of electronic states (DOS) of (a) BGDY, (b) V-BGDY, (c) Co-BGDY, and (d) Pd-BGDY, separated in spin-up (black color) and spin-down (red color) states. Blue and green regions correspond to the DOS projected on the TM atoms. **Supporting Fig. S12:** Density of electronic states (DOS) of (a) V_6 -GDY, (b) Co_6 -GDY, and (c) Pd_6 -GDY, separated in spin-up (black color) and spin-down (red color) states. Blue and green regions correspond to the DOS projected on the TM atoms. **Supporting Fig. S13:** Density of electronic states (DOS) of (a) V_6 -BGDY, (b) Co_6 -BGDY, and (c) Pd_6 -BGDY, separated in spin-up (black color) and spin-down (red color) states. Blue and green regions correspond to the DOS projected on the TM atoms. **Supporting Fig. S14:** Density of electronic states (DOS) of (a) V_6 , (b) Co_6 , and (c) Pd_6 , separated

in spin-up and spin-down states. **Supporting Table S1:** Adsorption energies of the second V, Co and Pd atom, respectively, on GDY. The configurations P1, P2 ... are shown in Figure S1. Adsorption energies are given in eV. **Supporting Table S2:** Adsorption energies of the third V, Co and Pd atom, respectively, on GDY. The configurations Pn ($n = 1, \dots, 7$) are shown in Fig. S2. Adsorption energies are given in eV. **Supporting Table S3:** Adsorption energies (in eV) of the third TM atom on a GDY layer with two pre-adsorbed TM atoms. Interatomic distances in Å. **Supporting Table S4:** Adsorption energies of the second individual TM atom on BGDY. Configurations P1, P2, and P3 are shown in Figure S5. Adsorption energies are given in eV. **Supporting Table S5:** Adsorption energies of the third individual TM atom on BGDY layer. The configurations P1, P2, P3 are shown in Fig. S6. Adsorption energies are given in eV. **Supporting Table S6:** Adsorption energies (in eV) of a third TM atom on BGDY with two pre-adsorbed TM atoms, for V, Co and Pd. Relevant interatomic distances are also reported. **Supporting Table S7:** Atomic Voronoi charges in clean GDY and BGDY, and for these layers with one V, one Co and one Pd atom adsorbed. A negative sign indicates a gain of electronic charge, while a positive sign indicates a loss. The labeled atoms (C1, C2, ...) are identified in Figure S9.